Supplement of

Trend and driving factors of dust soluble iron deposition to Northwest Pacific from East Asia during 2001-2017 springs

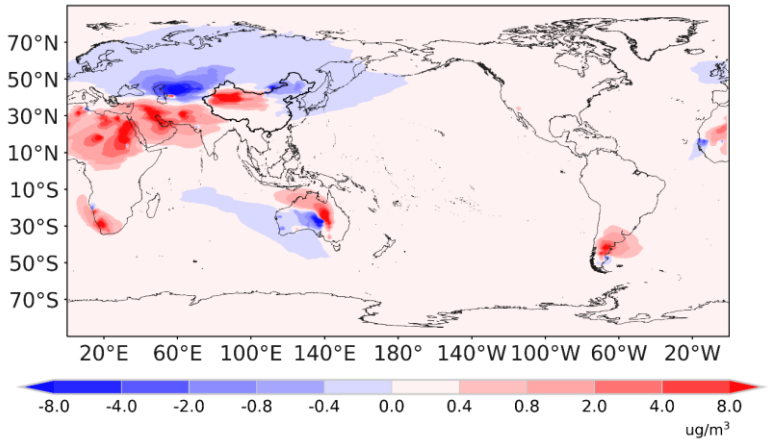

Figure S1. Compared to the default setting (3.5% iron in dust), changes in dust total iron surface concentrations from the developed model averaged 2001-2017 springs.

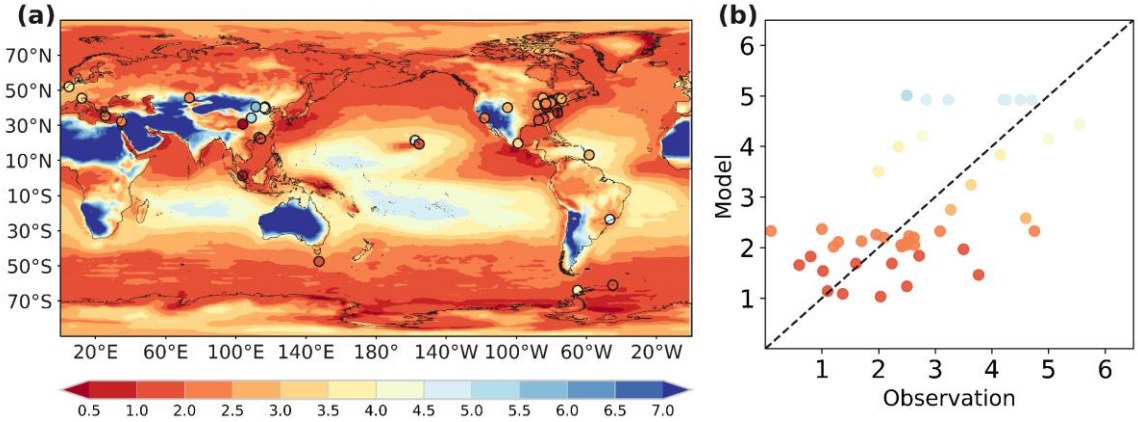

Figure S2. (a) Spatial distribution of aerosol pH in accumulation mode in 2013 and observed $PM_{2.5}$ pH (dots) from Pye et al. (2020). (b) The linear relationship between aerosol pH simulation and observed $PM_{2.5}$ pH.

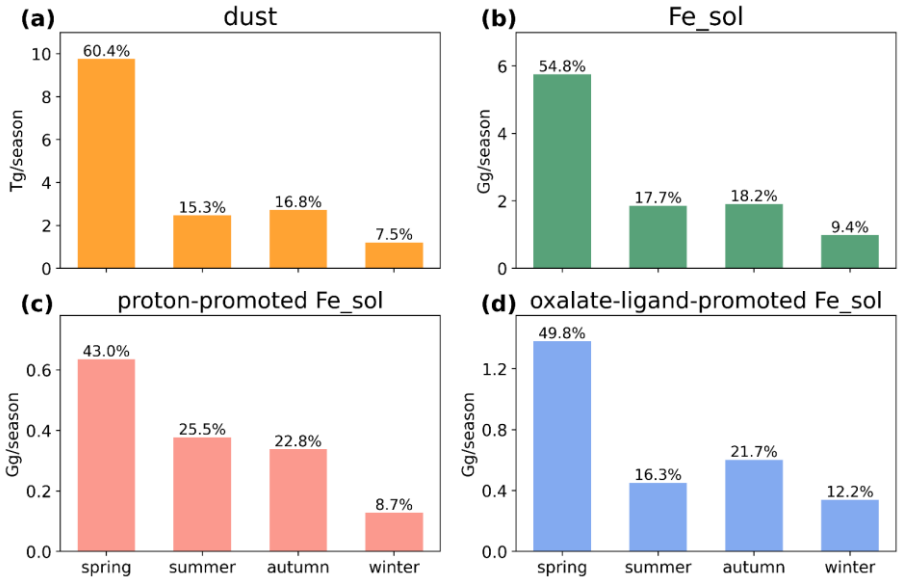

Figure S3. Dust, total soluble iron, proton-promoted soluble iron, and oxalate-ligand-promoted soluble iron deposition over Northwest Pacific (30-50N, 140E-160W) in 2001.

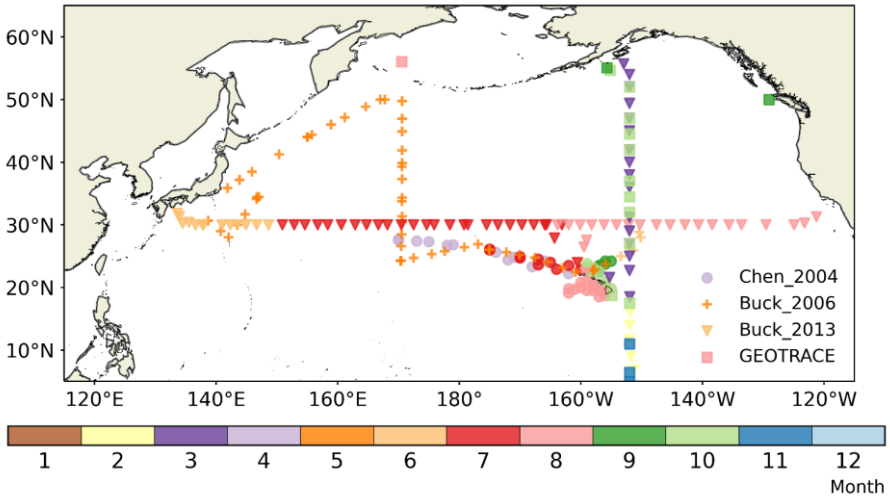

Figure S4. Months and locations of total and soluble iron observational samples over the North Pacific. Different colors represent different moths and different shapes represent different data sources (Chen et al., 2004; Buck et al., 2006; Buck et al., 2013; GEOTRACES).

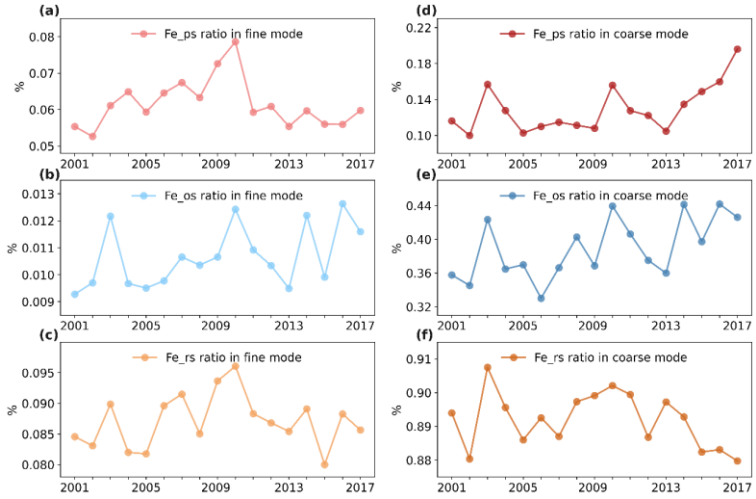

Figure S5. Temporal variations of the ratio of dust soluble iron deposition from proton-promoted (a, d), oxalate-ligand-promoted (b, e) and emissions (c, f) in coarse and fine mode (atiken + accumulation) to dust total iron deposition to the Northwest Pacific averaged of 2001-2017 springs.

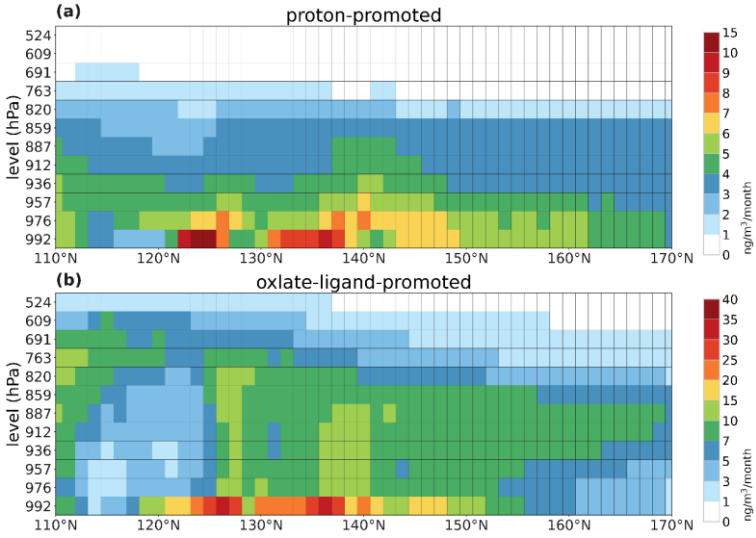

Figure S6. Vertical distributions of proton-promoted (a) and oxalate-ligand-promoted (b) soluble iron production rate averaged 30N-50N during the 2001-2017 springs.

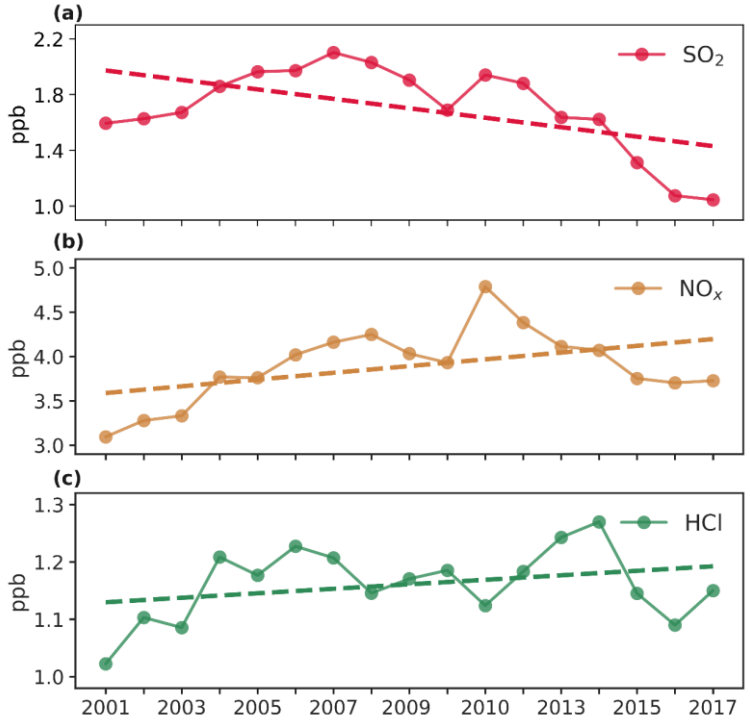

Figure S7. Temporal variations of surface concentrations of SO_2 (a), NO_x (a), and HCl (c) over the high production rate of proton-promoted soluble iron area (30-45N, 120-150E) averaged of 2001-2017 springs.

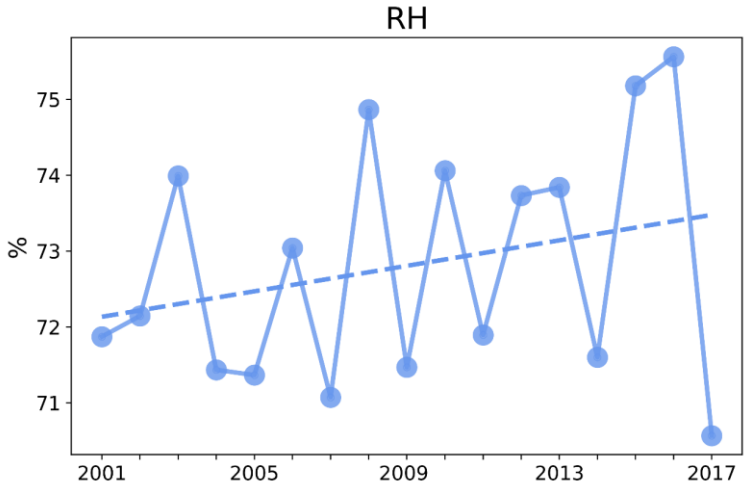

Figure S8. Temporal variations of simulated surface relative humidity over the high production rate of oxalate-ligand-promoted soluble iron area (30-45N, 120-150E) averaged of 2001-2017 springs.

References

Chen, Y.: Sources and fate of atmospheric nutrients over the remote oceans and their role on controlling marine diazotrophic microorganisms, Doctoral dissertation, available at: https://drum.lib.umd.edu/handle/1903/1967, 2004.

Buck, C. S., Landing, W. M., Resing, J. A., and Lebon, G. T.: Aerosol iron and aluminum solubility in the northwest Pacific Ocean: Results from the 2002 IOC cruise, Geochemistry, Geophysics, Geosystems, 7, https://doi.org/10.1029/2005GC000977, 2006.

Buck, C. S., Landing, W. M., Resing, J. A., and Measures, C. I.: The solubility and deposition of aerosol Fe and other trace elements in the North Atlantic Ocean: Observations from the A16N CLIVAR/CO2 repeat hydrography section, Marine Chemistry, 120, 57-70, https://doi.org/10.1016/j.marchem.2008.08.003, 2010.

GEOTRACES Intermediate Data Product Group (2023). The GEOTRACES Intermediate Data Product 2021v2 (IDP2021v2). NERC EDS British Oceanographic Data Centre NOC. doi:10.5285/ff46f034-f47c-05f9-e053-6c86abc0dc7e

Pye, H. O. T., Nenes, A., Alexander, B., Ault, A. P., Barth, M. C., Clegg, S. L., Collett Jr, J. L., Fahey, K. M., Hennigan, C. J., Herrmann, H., Kanakidou, M., Kelly, J. T., Ku, I. T., McNeill, V. F., Riemer, N., Schaefer, T., Shi, G., Tilgner, A., Walker, J. T., Wang, T., Weber, R., Xing, J., Zaveri, R. A., and Zuend, A.: The acidity of atmospheric particles and clouds, Atmos. Chem. Phys., 20, 4809-4888, 10.5194/acp-20-4809-2020, 2020.